Received: 11 January 2023 | Revised: 18 February 2023 | Accepted: 11 March 2023

DOI: 10.1002/htj.22852

ORIGINAL ARTICLE

HEAT TRANSFER WILEY

Thermal performance of dynamic, origami-inspired geometries: An experimental study

Farhan Ahmed | **Mehdi Khatamifar** | **Wenxian Lin** | **Rong Situ**

College of Science and Engineering, James Cook University, Townsville, Queensland, Australia

Correspondence
Mehdi Khatamifar, College of Science and Engineering, James Cook University, Townsville, QLD 4810, Australia.
Email: mehdi.khatamifar2@jcu.edu.au

Abstract

Origami has become an increasingly popular geometry in thermal engineering, namely, heat regulatory applications such as heat sinks and radiators. In this study, the radiative heating and radiative and natural convective cooling of three origami geometries (W-fold, Miura Ori (1), and Miura Ori (2)) made of heavy-duty aluminum foil under a radiative heater with different powers (800, 1600, and 2400 W) and different compression lengths (0.15, 0.25, 0.35, and 0.45 m) were investigated. It was found that the Miura Ori (1) and Miura Ori (2) geometries have three to four times high-temperature differences (the maximum temperature at the end of the heating process minus the initial temperature) than the W-fold geometry. The Miura Ori (2) and Miura Ori (1) geometries produced high heat capacity enhancements of 1.2–3.2 times at high compression lengths that showed great potential for applications such as solar steam generators. The overall heat transfer coefficient for cooling can be controlled by changing the compression length of the origami geometry, allowing for dynamic surface

temperature controls. This parameter decreases by up to 25.3%, 22.6%, and 45.9% for W-fold, Miura Ori (1), and Miura Ori (2), respectively, in comparison to their flat states.

KEYWORDS
apparent absorptivity, heat capacity enhancement, natural convection, origami, radiation

1 | INTRODUCTION

Origami is a form of paper-folding that originated in ancient Japan and has now become a common practice worldwide.[1] It is possible to use origami principles to create novel active systems. These systems can be assembled into complex three-dimensional (3D) arrangements and folded to provide active functionalities.[2–4] The shape-shifting and tunable properties of origami (the folding and unfolding motions) provide novel engineering applications. Many recent research topics in the application of origami are emerging such as batteries,[5] metamaterials,[6–8] smart materials,[9] and solar cells.[10]

Seymour et al.[11] developed an origami-based deployable ballistic barrier. The new origami-based ballistic barrier design provides benefits such as a large deployment ratio and a low degree of freedom with a large deployed surface area. Therefore, the deployment time is shorter and there is no need for external hardware to support the barrier. A zipper fashion was used for coupling rigidly foldable origami tubes made of thin stiff sheets by Filipov et al.[12] This arrangement significantly increases the stiffness of the assembly and provides only one flexible deformation mode that the system can deploy.

The Miura Ori fold is an auxetic (negative Poisson's ratio), flat, and rigid foldability with a single degree of freedom actuation. It has been implemented in a deployable solar panel array in the research vessel named space flight unit. This pattern is ideal for folding solar panels as it satisfies and conforms to the constraints of rigid and flat foldability. The origami flasher also has the potential to be used as a space solar panel. Unique properties of the flasher include its easily deployable shape and its static center, which has made it an attractive fold for this application, to be easily folded up during lift-off into a small volume, then deployed fully once in space.[13]

Origami also has been used as a means of reducing the weight and size of imaging devices currently in use by determining the most effective method of folding long focal length optics into smaller spaces.[1] This application is primarily seen in surveillance, telescopes, and cell phones. A particular application of optics and origami is the Eyeglass designed by Robert Lang, which is a foldable telescopic lens. The eyeglass is designed to be simply packed into a space shuttle and deployed in space by applying the principles of origami.[13]

3D biomedical structures in the form of particles, encapsulants, scaffolds, bioartificial organs, drug delivery tests as well as minimally invasive surgical tools have been implemented using origami.[14] Furthermore, new self-assembly techniques regulated by either heating or chemical stimulus, are being used to add to existing 3D tissue fabrication and patterning methods. There is a wide range of applications for origami in DNA structures and microbiology. A particular use of origami in this field is that of origami stents. These stents are used to enlarge clogged or weak arteries, veins, and colons.

The structure enters the body in its folded state, then at the appropriate location unfolds, hence supporting the body part and fulfilling its purpose.[13,15,16]

Several more applications using origami exist in the engineering world. Meta-materials are another application for active origami systems.[6,7,17–20] The Yoshimura fold (made up of a tessellation of diamonds, with either all-mountain or all-valley folds along the diagonals) for collapsible cylinders is being used to create antennas and other electronic applications.[21] This fold allows the frequency of each antenna to be tuned based on height, giving flexibility for communication requirements and storage in one's pocket. Another such application is the design of automobile airbags. The 3D shape of the airbag is vital in its effectiveness, which is derived from rigid origami and flat foldability to design the creases that would flatten the airbag. This allows the airbag to be folded into a compact state and to be rapidly unfolded in mere milliseconds, proving to be a lifesaving, injury-dampening device.[1]

There is tremendous potential for origami in thermal engineering due to its shape-shifting characteristics. NASA has been developing an unconventional, origami-inspired radiator that can fold and unfold.[22] This allows the radiator to control the temperature by altering the rate of heat loss/gain by performing shape-shifting maneuvers. The varying geometries can be achieved by implementing smart materials like temperature-sensitive materials[23] or shape-memory alloys.[24] The stimulus for temperature change can be from the spacecraft body (electronics temperature) or the absorption of heat from the earth and/or sun, causing a response from the radiator's geometry to alter to shed/conserve heat. The Miura Ori fold (V-groove cavity) has been investigated as the primary geometry, a fold that has already flourished in other engineering applications.[22]

Nevertheless, there is limited literature available on radiative heat transfer with origami geometries specifically. An experimental investigation was conducted by Lavery et al.[25] to benchmark the coupled radiation and conduction heat transfer modes. The experimental setup included a circular emitter, a square receiver, and a thermal imaging camera, surrounded by a blackbody open box. It is reported that the setup suffered heavily from daily ambient variations in the lab. This weakness in the setup was acknowledged and solved by Delpech et al.[26] who experimentally investigated the potential use of a radiative heat pipe for waste heat recovery in a ceramics kiln. Iverson et al.[27] conducted an analytical study in apparent absorptivity (the ratio between the geometry's heat flux to the heater's heat flux) of the standard V-groove fold, hinged V-groove, and the Miura Ori geometry. It is reported that for cases with the ratio of panel length to panel width less than 10, a finite length V-groove can be considered as an infinite V-groove model and this approximation error will be less than 5%. Regardless of the length ratio, the apparent absorptivity was found to decrease as the fold becomes flatter. A similar finding was also reported by Mulford et al.[28] and Wang and Jiang.[29] The possibility of using origami shape fins was investigated numerically by Wang and Jiang[29] for natural convection, forced convection, and radiation. It is reported that using origami increases active surfaces that rises the heat dissipation for radiation heat transfer. To confirm the theoretical findings reported by Wang and Jiang,[29] experimental studies were conducted by Grinham et al.[30] on both the back-and-forth fold and Miura Ori fold. It is reported that the W-fold and Miura Ori cooling rates were 55% and 67% higher than that of a flat geometry, respectively. Furthermore, a study of thermoelectric generators carried out by Akuto and Iwase[31] for curved heat sources found that for an origami-finned substrate, the (natural convection) heat transfer coefficient was 1.9 times higher than that of a flat substrate, whilst the finned substrate had a surface area 8 times larger than the flat substrate. In addition, it is reported that when the origami fin was contracted to 50% of its full length, the heat transfer coefficient was still 92% of a flat state's coefficient.

In light of current published studies, despite origami geometries discover going back many years and the possibility of implementing at dimensions that range from the nano to the meter scale with cross-disciplinary interest, there is limited work done on characterizing different origami geometries for heat transfer purposes due their complex geometries. The majority of available studies focus on one or two origami shapes for specific thermal arrangements. Future studies must investigate other origami shapes and the possibility of implementing them for thermal management applications to have a better view of the advantages and disadvantages.

The dynamic control of origami offers foldability and storage convenience, as well as tremendous thermal potential for applications such as solar steam generators or heat regulatory roles such as heat sinks or radiators. Due to little literature available on origami and their thermal behavior (heating/cooling), specifically the effect of origami width, this paper looks to fill the knowledge gap by exploring the thermal properties and performances of origami geometries at different widths. Three different origami patterns were seen to be popular geometries the standard V-groove (W-fold), the Miura Ori (1), and the Miura Ori (2). Thus, these three patterns, as well as a standard flat geometry, were experimentally studied to investigate radiative heating and the radiative and natural convective cooling properties at different stretching conditions.

2 | EXPERIMENTAL METHODOLOGY

The three selected geometries (W-fold, Miura Ori (1),[32] and Miura Ori (2) geometries) were first constructed using origami papers. W-fold and Miura Ori (1) were made of six folds and Miura Ori (2) is a variation of Miura Ori (1) with five vertical folds with 90° rotation. After the construction of the paper models, the same folding pattern was used for the aluminum foil models using 0.45×0.45 m pieces. It is decided that thick aluminum foils (35 microns) would be used to create hand-crafted models of the origami folds due to the extensive literature review on the thermal properties and design factors for heat sinks.[33] The details of fold patterns, schematic drawing, and final made geometries are illustrated in Figure 1.

The experimental setup used by Lavery et al.[25] was used for the present study. To prevent environmental radiation and ambient air variation, the experiments were conducted in a special room designed for dust tests (i.e., no air movement in the room). To further prevent air movement, barricades around the experimental rig were placed. Figure 2 shows the schematic of the experimental setup. The main parts of the experimental rig include a data logger (DataTaker 82E), a laptop with dEX2 software installed, two J-type thermocouples (Pacific Data Systems Australia), four retort stands to hold and adjust the width of the origami geometry and the thermocouples (two for the origami geometry and two for the thermocouples), a heater (Heller Quartz Indoor Radiant Heater), three origami (W-fold, Miura Ori (1) and Miura Ori (2)) geometries with aluminum foil and one flat sheet of aluminum foil, three barricades (matte black cardboard pieces) and one radiation shield ($0.6\ \text{m} \times 0.6\ \text{m} \times 0.01$ m plywood covered with aluminum foil). It was made sure that the geometry was aligned with the center of the heater.

The thermocouples were positioned to touch the surface as evenly as possible. One thermocouple was placed at the center of the foil to represent the entire geometries surface temperature, and the other around the outer edge of the foil to gauge the heat conductive properties of the foil. For all experiments conducted, the geometries and the heater were at a fixed distance of 0.18 m apart. It should be noted that for simplicity of the schematic, the barricades are not illustrated in Figure 2.

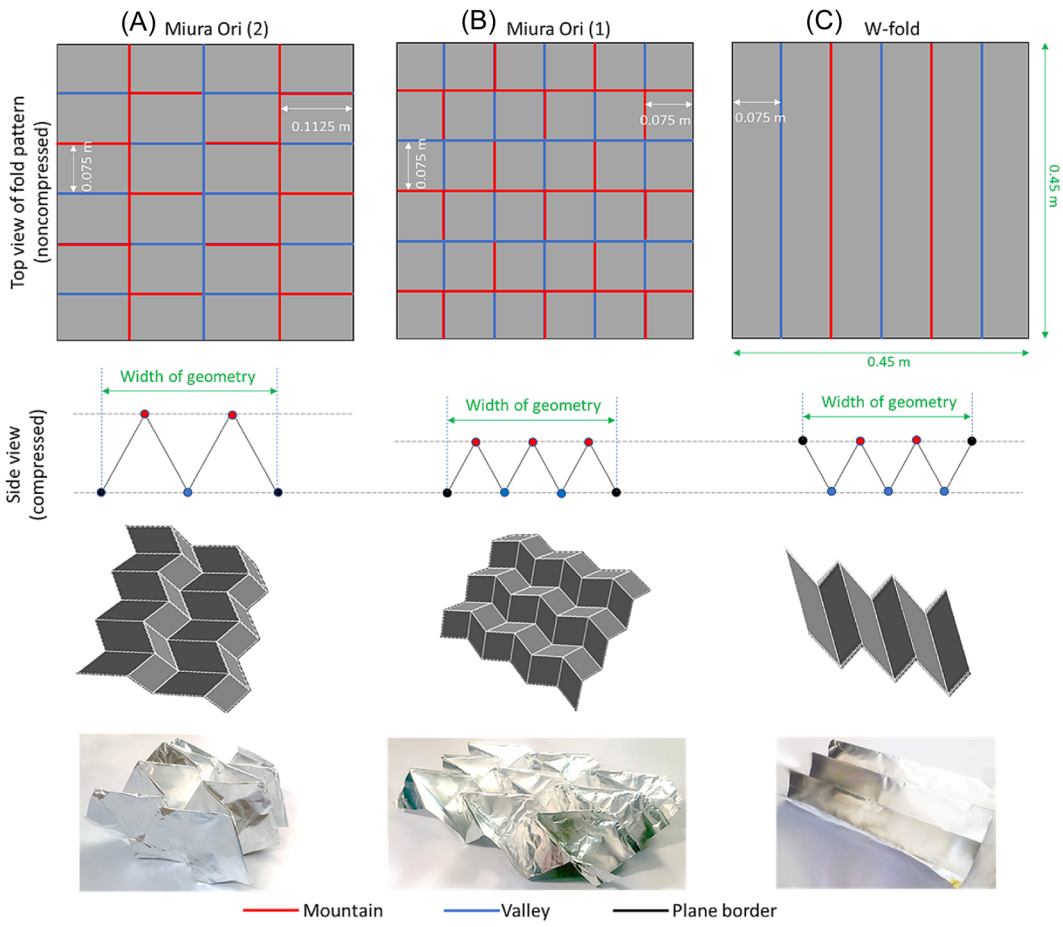

FIGURE 1 Paper and aluminum foil models of the origami designs used: (A) Miura Ori (2) geometry, (B) Miura Ori (1) geometry, (C) W-fold geometry. [Color figure can be viewed at wileyonlinelibrary.com]

For each geometry (W-fold, Miura Ori (1) and Miura Ori (2)), three geometry widths (geometry width of 0.15, 0.25, and 0.35 m) as can be seen for the case of W-fold in Figure 3, and for each geometry width, three different heater inputs (800, 1600, and 2400 W) were applied. Figure 4 presents the geometries and stand setup.

It should be noted that the power consumed by heat was assumed to be heater radiant power. In addition, one flat case (geometry width of 0.45 m) for the three power settings was added which made the total number of experiments to be 30. For the repeatability and reliability of the results, each test was repeated three times.

For the first stage of the experiment (heating via radiation), the heat shield was placed in front of the heater. Then the heater was turned on to one of the power inputs (800, 1600, 2400 W). The heat shield was removed after 90 s. The steady-state heating conditions were considered to be attained once the thermocouple's temperature variation was less than ±0.1°C and then the heater was turned off and quickly moved away. For the second stage of the experiment (cooling via radiation and natural convection), the thermocouple readings were recorded until they reached a steady state with a temperature variation of less than ±0.1°C for 20 s. An additional 180 s were recorded to ensure the room temperature reached the

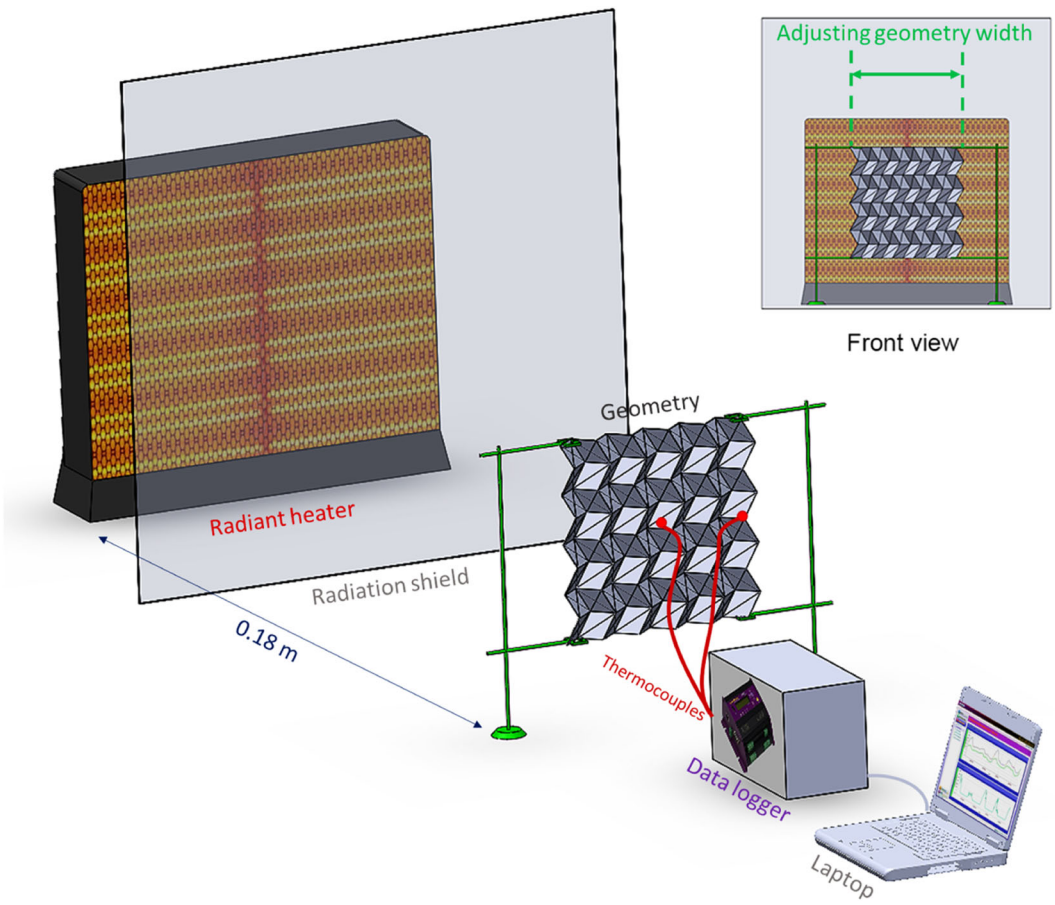

FIGURE 2 Schematic of the experimental setup. [Color figure can be viewed at wileyonlinelibrary.com]

steady-state conditions too. This process was repeated for different power inputs, geometries, and geometry widths (0.35, 0.25, and 0.15 m). Figure 5 presents a typical time series of the temperature for both the heating and cooling parts of the experiment for the case of Miura Ori (2), 2400 W, and a geometry width of 0.15 m.

From the time series of the temperature obtained, the maximum temperature difference of the geometry is extracted, which occurs at the time when the heating stage ends and the cooling stage commences. The total heat absorbed by the geometry is given as:

$$Q_{\text{rec}} = mC\Delta T, \tag{1}$$

where m is the mass of the aluminum foil, C is the specific heat capacity of aluminum foil, and ΔT is the maximum temperature difference. In addition, to find the total energy received/enhanced by a surface ($Q_{\text{rec,origami}}$) compared to its flat state ($Q_{\text{rec,flat}}$), the heat capacity enhancement is defined as the ratio between the heat absorbed by the compressed origami geometry to its flat case (0.45 m), for the same heater power (a geometry is considered to be compressed when its width is less than 0.45 m which is the flat foil size):

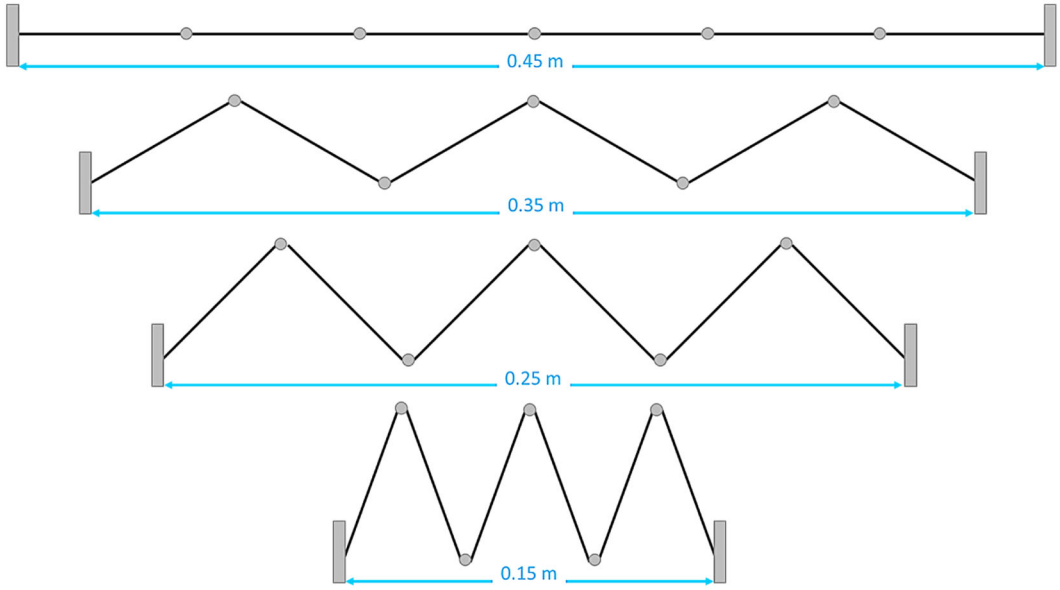

FIGURE 3 Geometry width variations. [Color figure can be viewed at wileyonlinelibrary.com]

$$\epsilon = \frac{Q_{\text{rec,origami}}}{Q_{\text{rec,flat}}}. \tag{2}$$

A common parameter used in origami radiation is the apparent absorptivity (α_a), which is the ratio between the geometry's heat flux to the heater's heat flux, defined as follows:

$$\alpha_a = \frac{q_{\text{h,foil}}}{q_{\text{heater}}}, \tag{3}$$

where the subscript h represents the heating stage, $q_{\text{h,foil}}$, and q_{heater} are the heat fluxes of the foil and the heater that can be calculated by dividing the heat transfer rate by its surface area (A_s, projected surface area). For the cooling down stage, the steady-state cooling temperature, $T_{\text{c,ss}}$ is defined as the 95% mark between the hot surface (T_{hot}) and the room temperature (T_{room}), as follows:

$$T_{\text{c,ss}} = T_{hot} - 0.95(T_{\text{hot}} - T_{\text{room}}). \tag{4}$$

Based on the steady-state cooling temperature ($T_{\text{c,ss}}$), the initial cooling temperature (i.e., the temperature at which the geometry has reached after the steady-state heating, T_{hot}), and the time taken to reach the steady-state cooling temperature ($t_{\text{c,ss}}$), the cooling heat flux was calculated as follows:

$$q_{\text{c}} = \frac{mC(T_{\text{hot}} - T_{\text{c,ss}})}{A_s t_{\text{c,ss}}}, \tag{5}$$

where the subscripts c and ss represent the cooling stage and the steady state, respectively.

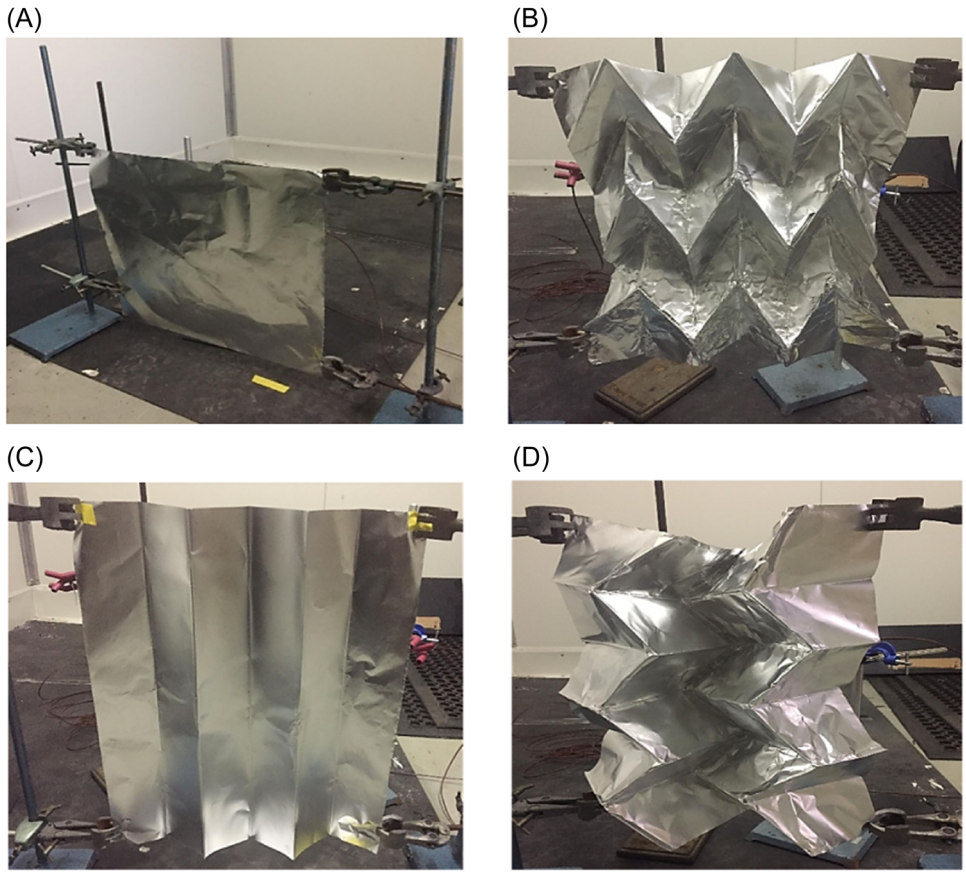

FIGURE 4 Geometry and stand setup (A) flat case, (B) Miura Ori (1), (C) W-fold, and (D) Miura Ori (2). [Color figure can be viewed at wileyonlinelibrary.com]

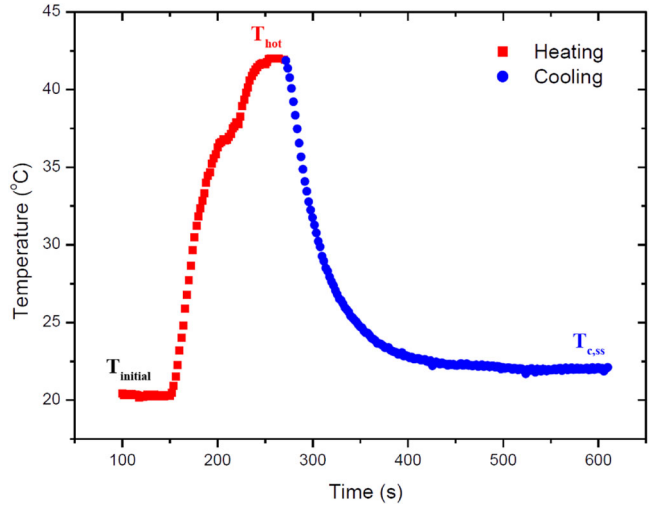

FIGURE 5 A typical time series of the temperature for both the heating and cooling stages of the experiment for the case of Miura Ori (2), 2400 W, and geometry width of 0.15 m. [Color figure can be viewed at wileyonlinelibrary.com]

TABLE 1 The maximum uncertainty of the main parameters.

Parameter	Maximum Uncertainty
Temperature	±0.1°C
Mass	±0.0005 kg
Time	±1 s
Specific heat capacity	±10 J/kgK
Heater power	±5%
Length	±1 mm

The maximum uncertainty of the main parameters of this study is presented in Table 1. An error analysis with these data was conducted and it was found that the overall maximum probable error calculated for the heat flux of W-fold, Miura Ori (1), and Miura Ori (2) geometries is 7.37%, 5.54%, and 5.40%, respectively.

3 | RESULTS AND DISCUSSION

3.1 | Radiative heating

Figure 6 presents temperature differences of geometries against the width of geometry for different thermal loads from the heater. The temperature difference is the difference between the steady-state heating temperature and the initial temperature of the surface. Note that 0.45 m of width is the flat state.

In general, the temperature difference increased with increasing compression across the three heat loads. The biggest temperature differences were observed at the most compressed state of 0.15 m consistently across all geometries and heater inputs. In comparison to the flat case, temperature increases of 235%, 194%, and 62.6% were observed for the Miura Ori (2), Miura Ori (1), and W-fold, respectively. The Miura Ori (1) and Miura Ori (2) showed three to four times high-temperature differences than the W-fold. In addition, increasing heater intensities also led to higher temperature differences across the three geometries, as expected. From 800 to 2400 W at 0.15 m compression, the temperature difference increased by factors of 2.08, 2.04, and 1.87 for the W-fold, Miura Ori (1), and Miura Ori (2) patterns, respectively. Interestingly, when analyzing each heater input, the lowest heat input produced the largest percentage increase in temperature difference, compared to the flat 0.45 m case. These results showed that origami geometries are more efficient and capable of absorbing and retaining radiative heat than their flat case for the same heat intensity, with the surface area of all geometries kept constant. The cavity effect is visible in these plots.

It should be noted that cavities (created by origami folds) are important characteristics of origami that concentrate emission from all internal surfaces to the cavity opening. Therefore, the cavity emission is highly directional, allowing for control of directional radiative heat transfer and deep cavities can result in near-blackbody behavior.[28,34–36] As the compression increases, the cavities get deeper thus trapping more radiation and increasing radiation reabsorption. Geometry and compression have less effect on surface temperature for higher radiation inputs as smaller temperature increases were observed. The W-fold is one of the most

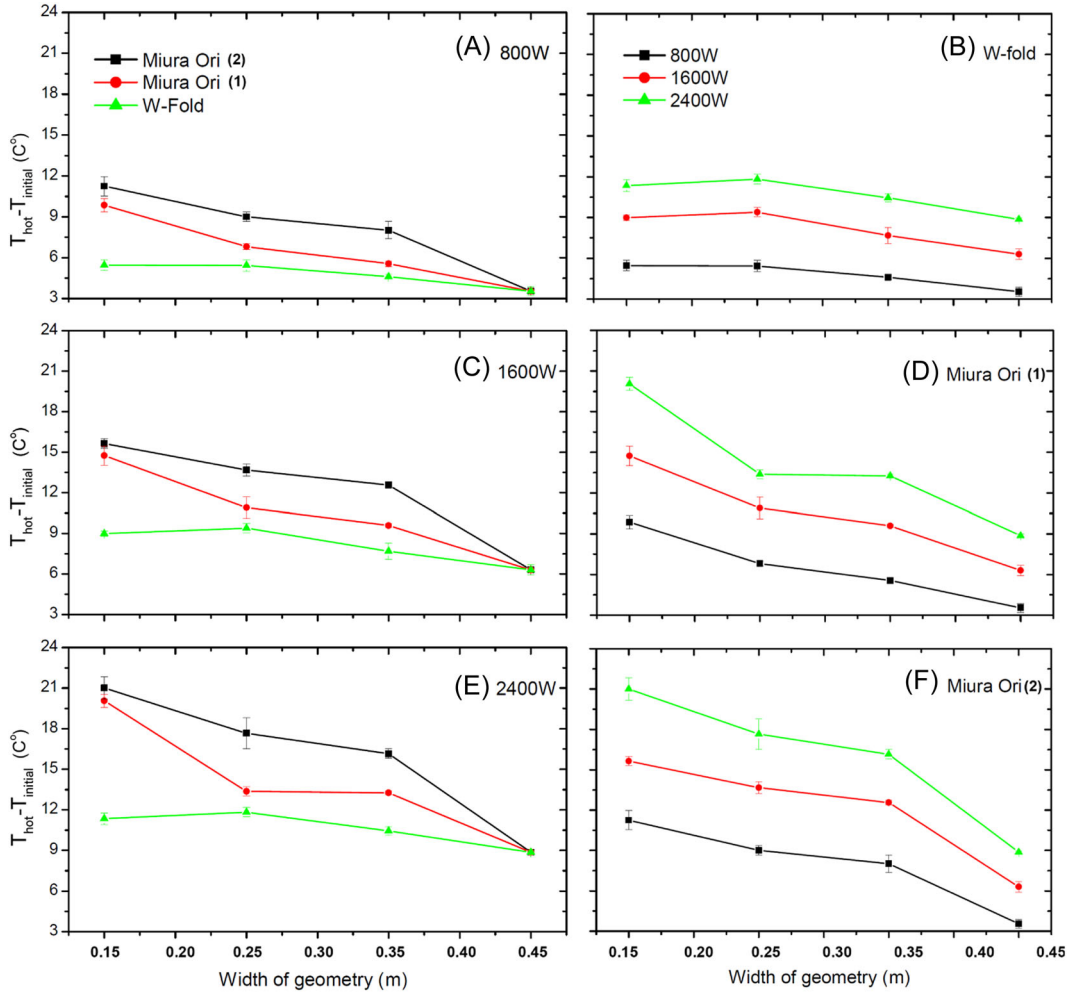

FIGURE 6 Temperature difference of geometries against the width of geometry for different thermal loads from the heater. [Color figure can be viewed at wileyonlinelibrary.com]

studied geometries[27,28] and the temperature is expected to continue to increase, as it has from 0.45 to 0.25 m for the 1600 and 2400 W trials. Due to the nature of aluminum foil, being easily deformed, and the nature of the W-fold having long folded columns, it is likely that the structure became less rigid/straight as the geometry was compressed. Unlike in numerical studies, where geometries can be kept rigid and straight, the flimsy nature of the foil W-fold may have led to a reduced cavity depth, thereby reducing the trapped radiation in the cavity and consequently lowering the temperature difference at small widths.

From the comparisons between the geometries in Figure 6 (left column), it is clear the Miura Ori (2) produces the highest surface temperatures consistently throughout all heater settings and compressions. In terms of temperature difference per meter of compression:

$$\Delta T_{\text{W-fold}} < \Delta T_{\text{Miura Ori (1)}} < \Delta T_{\text{Miura Ori (2)}}. \tag{6}$$

The Miura Ori (1) however produced temperature differences close to the Miura Ori (2) pattern for 15 cm of compression, regardless of heater setting. The W-fold produced the weakest temperature difference. For example, at 0.15 m compression and 2400 W intensity, the W-fold produced a temperature difference of 11.35°C, whereas the Miura Ori (1) and Miura Ori (2) patterns produced temperature differences of 20.1°C and 21.0°C, respectively. This effect was also reported by Iverson et al.[27] The open-ended nature of the W-fold geometry causes higher heat loss. The Miura Ori (1) does not have deep cavities compared to W-fold but has more, smaller, and closed cavities, thus maximizing the cavity effect, leading to higher temperature differences.

The heat transfer rate enhancement (Equation 2) is a useful parameter for the applications such as solar steam generators, solar panels, or space radiators. Figure 7 presents results for the heat transfer rate enhancement against the width of geometry for different thermal loads from the heater.

As the heat enhancement factor is defined as the ratio of heat transfer between compressed origami and a straight surface, an enhancement value of one means the same amount of energy was absorbed as the flat case of 0.45 m width, for the same heater input. Generally, there was an

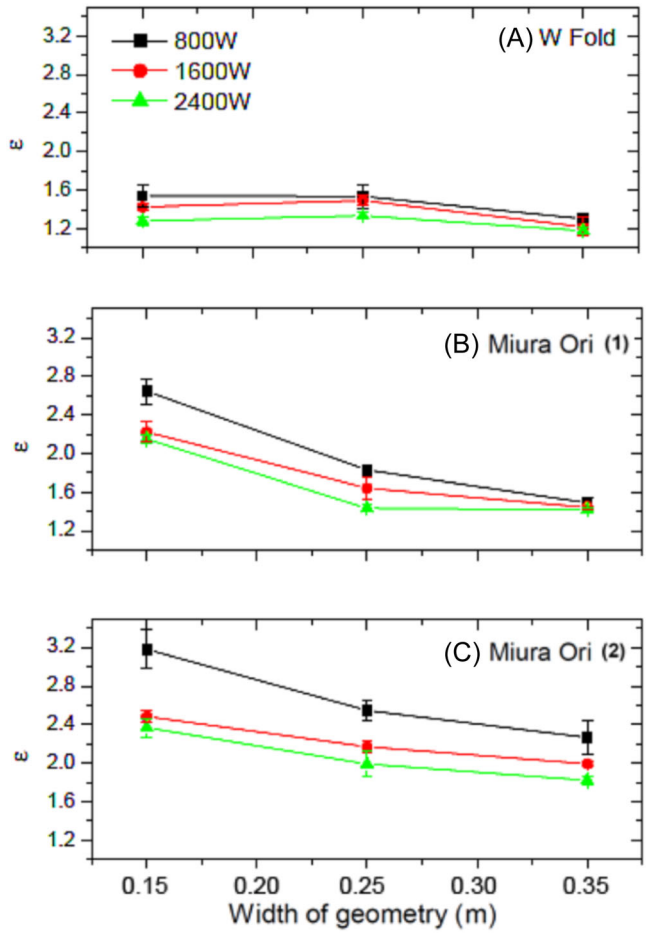

FIGURE 7 Heat capacity enhancements of origami shapes against the width of geometry for different thermal loads from the heater. [Color figure can be viewed at wileyonlinelibrary.com]

increase in enhancement with increasing compression (or decreasing width), which is especially apparent in the Miura Ori (1) and Miura Ori (2) patterns. Figure 7 reiterated the findings from Figure 6 that lower intensities led to higher enhancement ratios for all geometries. Geometries that were compressed (width <0.45 m) all resulted in enhancement values larger than one. Enhancement values of 1.54, 2.65, and 3.18 were found for the W-fold, Miura Ori (1), and Miura Ori (2) patterns, respectively, for the 800 W tests at 15 cm width, which indicates that lower heat intensities led to increased enhancements. For the same compression but at 2400 W intensity, enhancement values of 1.28, 2.15, and 2.37 were found for the W-fold, Miura Ori (1), and Miura Ori (2) patterns, respectively. The results showed that origami geometries with cavities will absorb more energy than their flat case for the same heater input. In addition, the width of the geometry and enhancement value shows a negative correlation (decreasing width increases the enhancement). The cavity effect is displayed as higher compressions, which lead to deeper cavities of smaller openings, trapping radiation and causing increased scattering and reabsorption, leading to higher temperatures (than a flat case) and consequently enhancement values of greater than 1.

It can be seen that depending on the shape, the heat absorption enhancement achieved using origami ranged from 1.2 to 3.2 and the Miura Ori (2) and Miura Ori (1) produced high enhancements at high compressions. These findings have great potential in applications such as solar steam generators to help mitigate the energy and water crisis. For instance, Hong et al.[37] used highly compressed origami geometries employing solar radiation to produce clean water and reported increased efficiency.

Comparison of geometry and source heat fluxes is a common practice in literature for general radiative heat studies. Dividing the heat flux of the geometry by that of the heater yields the dimensionless apparent absorptivity (α_a). The angle of incidence and the nature of the irradiation into the cavity has a significant effect on the apparent absorptivity of a cavity.[38] There is radiation loss from the heater to the origami, which depends on the distance between them, hence the use of view factors in the calculation is necessary. However, due to a lack of literature available for view factors of origami geometries and their complexity, it was decided to fix the distance between the heater and geometries. This would ensure a fair comparison, and thus the heating heat flux (and consequently view factor) would only be a function of the origami shape rather than the position of the heater. Figure 8 presents the effect of origami width on the geometry's apparent absorptivity for various heater intensities.

It can be seen that increasing compression increased the apparent absorptivity for W-fold and Miura Ori (2) from 0.35 to 0.15, Miura Ori (1). This outcome was also reported by other researchers.[27,28] The Miura Ori (1) fold best showed this trend, whereas the W-fold and Miura Ori (2) patterns generally supported these findings. For 800 W, the increase in apparent absorptivity between 0.45 and 0.15 m was found to be 16.3%, 79.6%, and 68.4%, for the W-fold, Miura Ori (1), and Miura Ori (2), respectively. However, for the 800 W case in Figure 8C, an increase of 70.1% was observed when comparing 0.35 m to the flat case. The results show that the origami geometries are more efficient at absorbing and retaining radiative heat than its flat case, for the same heater input. This is especially impressive when origami geometries have less width than the flat case, meaning less radiation is received from the heater, than a flat case. Even then the origami geometries absorb and retain heat better than the 0.45 m case.

The heat flux of the geometry (which is proportional to the apparent absorptivity) is proportional to the temperature difference between the surface and surroundings and inversely proportional to the time taken to reach steady-state conditions. Increasing compression (or decreasing width) has led to an increase in temperature difference but also an increase in

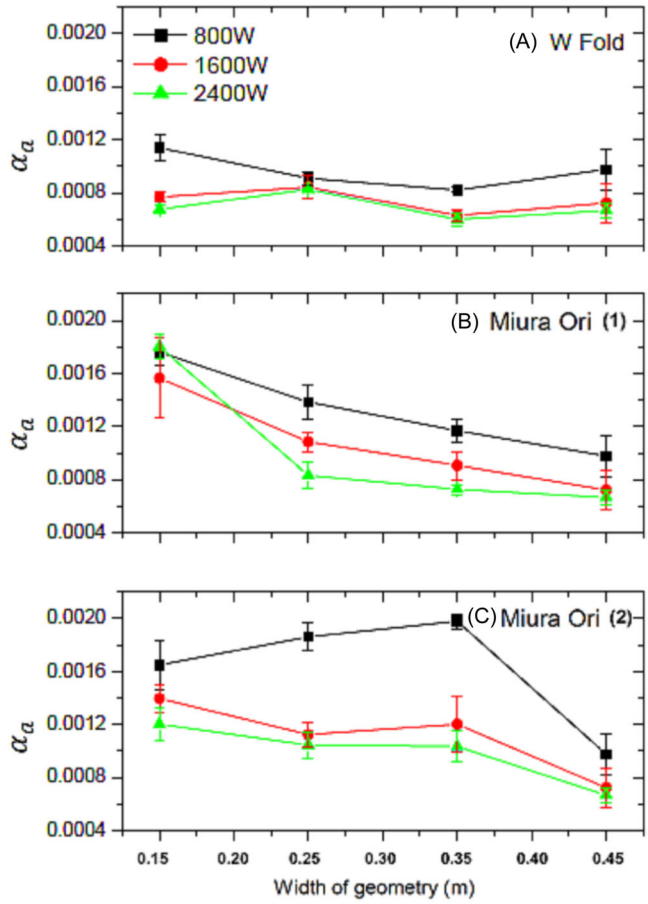

FIGURE 8 Apparent absorptivity of origami shapes against the width of geometry for different thermal loads from the heater. [Color figure can be viewed at wileyonlinelibrary.com]

steady-state time. Thus, the apparent absorptivity is balanced by the temperature difference and time to steady-state. This means that a small temperature difference and/or a long time to steady-state conditions lead to decreased apparent absorptivity. This explains why there are decreases in apparent absorptivity for widths less than 45 cm, namely, the 800 W test in Figure 8C. When the time series of temperature for the heating stage was investigated (sample data in Figure 5), it was observed that geometries with deeper cavities generally required the longest time to reach steady-state conditions, which would suggest smaller heat flux values. For instance, examining the case of 1600 W for the Miura Ori (2) pattern at 0.35 and 0.15 m compression shows that for the 0.35 m case, the average time to steady-state cooling was 80 s, and for the 0.15 m case the time to steady-state on average was 153 s. This fine balance between apparent absorptivity and compression was also reported by Iverson et al.[27]

For W-fold geometry, a numerical study conducted by Iverson et al.[27] has revealed that the apparent absorptivity of this geometry decreases with increasing compression approximately 90°–120° (which are equivalent to 0.32 and 0.39 m compression, respectively). A similar trend (reduction in the apparent absorptivity from 0.45 to 0.35 m) can be identified for the W-fold in Figure 8A. The reason for the loss of apparent absorptivity for the initial compression values

may be due to end effects. Additional losses are possible due to the uncapped/open ends of the vertical trenches of the W-fold. As a result, the cavity effect decreases as radiation may escape without scattering inside the cavity. A similar effect can be seen for the Miura Ori (1) fold as the apparent absorptivity of the Miura Ori (1) increased with increasing compression which is in agreement with numerical results by Iverson et al.[27]

Experimental results of this study and numerical data from literature[27] prove the cavity effect of radiative reabsorption and entrapment, leading to a higher apparent absorptivity than a flat case. For the Miura Ori (2) fold (which is a variation of the Miura Ori (1) but oriented differently), except for the 800 W case, the same analysis could be conducted that also agrees with Iverson et al.[27] Miura Ori results.

3.2 | Radiative and natural convective cooling

The second part of this study is the cooling down of the geometries after reaching steady-state heating conditions. The geometries were allowed to cool by natural convection and radiation after the heater was turned off. Figure 9 presents results for cooling heat flux of origami shapes against the width of geometry for different thermal loads from the heater.

It is expected to have a general increase in cooling heat flux with compression if the cooling temperature difference dominates cooling time. A small heat flux suggests a long cooling time and/or a small temperature difference between the surface and surroundings. In general, the cooling heat flux increased with compression, though complicated trends are identified. Furthermore, increasing heater input also increased cooling heat flux, as a larger heater input increased the temperature difference between the surface and surroundings.

For the W-fold case (Figure 9A), the cooling heat flux generally shows little influence by origami width. The 800 and 1600 W settings show similar trends and the cooling heat flux increased with compression. For 2400 W, the largest cooling heat flux occurred at the flat state, opposite to the 800 and 1600 W trends. It is hypothesized that, due to higher heating intensities, the geometry had a large temperature difference, and during the cooling stage, there was more reabsorption for flat surfaces via radiation and natural convection inside the cavities compared to 1600 and 800 W tests. Thus, for the 2400 W test, higher compressions intensity led to increased cavity effect phenomenon, leading to larger cooling times required to reach steady-state, and thus a lower heat flux than its 0.45 m width.

The Miura Ori (1) (Figure 9B) displays a consistent trend of increasing cooling heat flux with compression. Cooling heat flux rates, when compared to a flat case, were found to increase by 131%, 81.2%, and 57.5% for the 800, 1600, and 2400 W, respectively. A similar trend was found in Section 3.1 where lower heat intensities led to high heat absorption enhancements, compared to the flat case. The results suggest that compressing the Miura Ori (1) fold does not detriment the cooling mechanisms that are an important characteristic of heat sinks and radiators. Increased compression led to increased surface temperatures. Thus, Miura Ori (1) exhibits properties of attaining and losing heat in a balanced manner.

The Miura Ori (2) cooling heat flux performance also produced a consistent trend between heater settings. At 0.35 m width, there appeared to be a maximum cooling heat flux. An optimum width for maximum cooling is suggested by this finding. From flat (0.45 m) to 0.35 m width, cooling rates were increased by factors of 2.54, 2.04, and 1.67 for the 800, 1600, and 2400 W tests, respectively. Furthermore, from 0.35 to 0.15 m, cooling rates decreased by 25.9%, 35.3%, and 25.1% for 800, 1600, and 2400 W tests, respectively. Compressions past 0.35 m led to

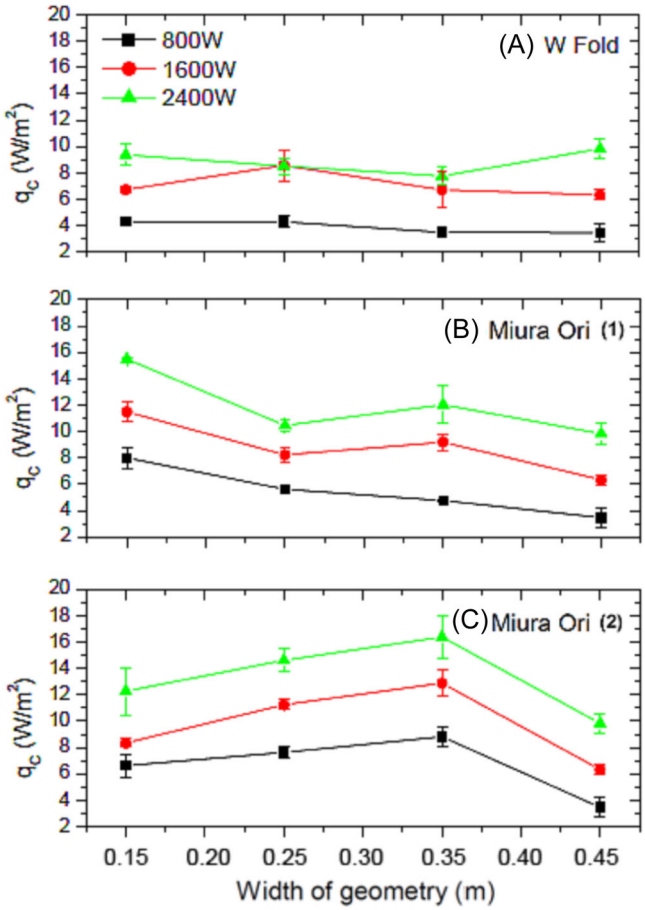

FIGURE 9 Cooling heat flux of origami shapes against the width of geometry for different thermal loads from the heater. [Color figure can be viewed at wileyonlinelibrary.com]

weaker cooling heat fluxes. In addition, high-temperature differences were observed for the 35 cm case for the Miura Ori (2) in Section 3.1, contributing to the high cooling heat flux seen. As stated already these results suggest that the cooling rates can be maximized at 0.35 m of compression as well as minimized at 0.15 or 0.45 m of compression, offering great dynamic flexibility that a flat geometry could not provide. Due to deeper cavities at greater compressions, the cooling time to steady-state became longer and reduced cooling heat flux.

Due to a lack of research on the cooling mechanisms of origami, comparisons cannot be made to the literature. Grinham et al.[30] investigated the cooling of origami geometries (W-fold and Miura Ori (2)) when they are perpendicular to the direction of gravity (horizontal). It was reported that the cooling heat flux of the W-fold and Miura Ori (2) increased by 55% and 67%, respectively.

To investigate the cooling heat flux of origami shapes, Figure 10 presents the cooling heat flux of origami shapes against the temperature difference (the temperature difference between surface and surrounding) for different geometry widths at different heat fluxes. As compressions increase, the gradient of the lines (which represent the overall heat transfer coefficient, h) decreases. For a 0.35 m stretch, it seems that the W-fold has the lowest h value, followed by the Miura Ori (1) for 0.25 m and then Miura Ori (2) for 0.15 m. Thus, for the case of

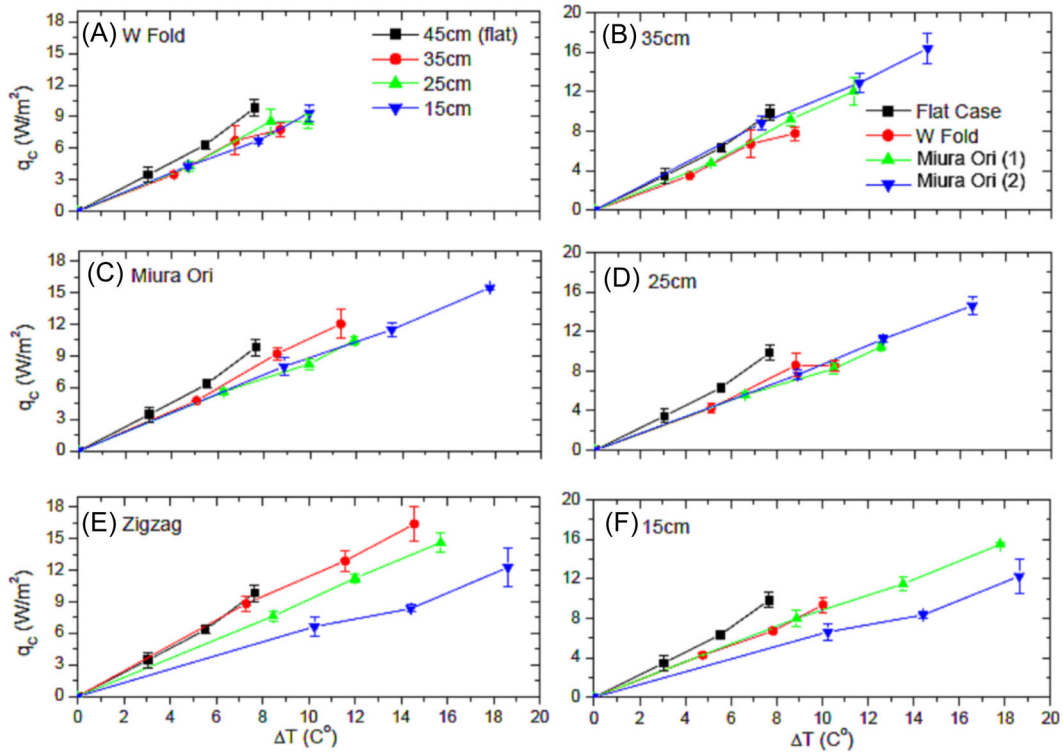

FIGURE 10 Cooling heat flux of origami shapes against the width of geometry for different thermal loads from the heater. [Color figure can be viewed at wileyonlinelibrary.com]

static designs, the results from Figure 10 can aid in the selection of geometry based on the design requirement.

For all geometries, the highest heat transfer coefficient occurred at 45 cm (flat case). The decrease in this coefficient between 0.45 and 0.15 m was found to be 25.3%, 22.6%, and 45.9% for the W-fold, Miura Ori (1), and Miura Ori (2), respectively. Considering how the cavities become deeper with increasing compression, and larger air resistance due to narrower trenches which reduce air free flow rate, it is expected for there to be less heat transferred from the surface to the surrounding. The findings suggest that the heat loss to surroundings can be significantly limited by simply compressing the geometry, thus increasing heat retention better than a flat case. The nature of the Miura Ori (1) and Miura Ori (2), unlike the W-fold, do not allow for hot air to rise, which is the mode of heat transfer in natural convection. Consequently, the overall heat transfer coefficient decreases with increasing compression.

4 | CONCLUSIONS

To examine the radiative heating and radiative and natural convective cooling of the origami, three origami geometries (W-fold, Miura Ori (1), and Miura Ori (2)) were made of heavy-duty aluminum and placed under a radiative heater (800, 1600, and 2400 W) with different compression length (15, 25, 35, and 45 cm).

The key findings of the present study can be summarized as follows:

- Origami geometries can increase the surface temperature under the same illumination by up to a factor of 3.2 compared to a flat case of the same surface area and material.
- Superior surface temperatures and heating rates are achieved with increasing compression (or cavity depth) than a flat geometry.
- Origami geometries are better at retaining heat at high cavity depths (compressions) than flat cases.
- The overall heat transfer coefficient for cooling can be controlled by changing the compression of the origami, allowing for dynamic surface temperature controls.
- Overall heat transfer coefficient decreases by up to 25.3%, 22.6%, and 45.9% for W-fold, Miura Ori (1), and Miura Ori (2), respectively, in comparison to their flat states.
- Dynamic geometries can allow for complete control of thermal properties for heating and cooling by simply changing the width of the geometry.

ACKNOWLEDGEMENT

Open access publishing facilitated by James Cook University, as part of the Wiley - James Cook University agreement via the Council of Australian University Librarians.

ORCID

Mehdi Khatamifar https://orcid.org/0000-0001-6273-7655
Wenxian Lin https://orcid.org/0000-0001-5264-2097

REFERENCES

1. Turner N, Goodwine B, Sen M. A review of origami applications in mechanical engineering. *Proc Inst Mech Eng C J Mech Eng Sci*. 2016;230(14):2345-2362.
2. Felton S, Tolley M, Demaine E, Rus D, Wood R. A method for building self-folding machines. *Science*. 2014;345(6197):644-646.
3. Rus D, Tolley MT. Design, fabrication and control of origami robots. *Nat Rev Mater*. 2018;3(6):101-112.
4. Sareh P, Chen Y. Intrinsic non-flat-foldability of two-tile DDC surfaces composed of glide-reflected irregular quadrilaterals. *Int J Mech Sci*. 2020;185:105881.
5. Song Z, Wang X, Lv C, et al. Kirigami-based stretchable lithium-ion batteries. *Sci Rep*. 2015;5:10988.
6. Lv C, Krishnaraju D, Konjevod G, Yu H, Jiang H. Origami based mechanical metamaterials. *Sci Rep*. 2014;4:5979.
7. Zhai Z, Wang Y, Wang Y. Origami-inspired, on-demand deployable and collapsible mechanical metamaterials with tunable stiffness. *Proc Natl Acad Sci U S A*. 2018;115(9):2032-2037.
8. Silverberg JL, Evans AA, McLeod L, et al. Using origami design principles to fold reprogrammable mechanical metamaterials. *Science*. 2014;345(6197):647-650.
9. Tolley MT, Felton SM, Miyashita S, Aukes D, Rus D, Wood RJ. Self-folding origami: shape memory composites activated by uniform heating. *Smart Mater Struct*. 2014;23:094006.
10. Tang R, Huang H, Tu H, et al. Origami-enabled deformable silicon solar cells. *Appl Phys Lett*. 2014;104(8):083501.
11. Seymour K, Burrow D, Avila A, et al. Origami-based deployable ballistic barrier. *Origami7*. 2018;3:763-778.
12. Filipov ET, Tachi T, Paulino GH. Origami tubes assembled into stiff, yet reconfigurable structures and metamaterials. *Proc Natl Acad Sci U S A*. 2015;112(40):12321-12326.
13. Debnath S, Fei L. Origami theory and its applications: a literature review. *World Acad Sci Eng Technol*. 2013;73:1131-1135.
14. Randall CL, Gultepe E, Gracias DH. Self-folding devices and materials for biomedical applications. *Trends Biotechnol*. 2012;30(3):138-146.
15. Zhu Y, Birla M, Oldham KR, Filipov ET. Elastically and plastically foldable electrothermal micro-origami for controllable and rapid shape morphing. *Adv Funct Mater*. 2020;30:2003741.
16. Breger JC, Yoon C, Xiao R, et al. Self-folding thermo-magnetically responsive soft microgrippers. *ACS Appl Mater Interfaces*. 2015;7(5):3398-3405.

17. Yang N, Silverberg JL. Decoupling local mechanics from large-scale structure in modular metamaterials. *Proc Natl Acad Sci U S A*. 2017;114(14):3590-3595.
18. Li S, Fang H, Sadeghi S, Bhovad P, Wang KW. Architected origami materials: how folding creates sophisticated mechanical properties. *Adv Mater*. 2019;31(5):1805282.
19. Fang H, Chu SCA, Xia Y, Wang KW. Programmable self-locking origami mechanical metamaterials. *Adv Mater*. 2018;30(15):1706311.
20. Schenk M, Guest SD. Geometry of Miura-folded metamaterials. *Proc Natl Acad Sci U S A*. 2013;110(9):3276-3281.
21. Yao S, Georgakopoulos SV, Cook B, Tentzeris M. A novel reconfigurable origami accordion antenna. Paper presented at: 2014 IEEE MTT-S International Microwave Symposium (IMS2014). IEEE;2014:1-4.
22. Jenner L. NASA's new shape-shifting radiator inspired by Origami. 2017. https://www.nasa.gov/feature/goddard/2017/nasa-s-new-shape-shifting-radiator-inspired-by-origami
23. Leong TG, Randall CL, Benson BR, Bassik N, Stern GM, Gracias DH. Tetherless thermobiochemically actuated microgrippers. *Proc Natl Acad Sci U S A*. 2009;106(3):703-708.
24. Bassik N, Stern GM, Gracias DH. Microassembly based on hands free origami with bidirectional curvature. *Appl Phys Lett*. 2009;95(9):091901.
25. Lavery NP, Vuji MR, Brown SGR. Thermal experimental investigation of radiative heat transfer for the validation of radiation models. *WIT Trans Model Simul*. 2005;41:251-261.
26. Delpech B, Axcell B, Jouhara H. Experimental investigation of a radiative heat pipe for waste heat recovery in a ceramics kiln. *Energy*. 2019;170:636-651.
27. Iverson BD, Mulford RB, Lee ET, Jones MR. Adaptive net radiative heat transfer and thermal management with origami-structured surfaces. Paper presented at: 16th International Heat Transfer Conference. 2018.
28. Mulford RB, Jones MR, Iverson BD. Dynamic control of radiative surface properties with origami-inspired design. *J Heat Transfer*. 2015;138(3):032701.
29. Wang X, Jiang H. Design of origami fin for heat dissipation enhancement. *Appl Therm Eng*. 2018;145:674-684.
30. Grinham J, Craig S, Ingber DE, Bechthold M. Origami microfluidics for radiant cooling with small temperature differences in buildings. *Appl Energy*. 2020;277:115610.
31. Akuto M, Iwase E. An origami heat radiation fin for use in a stretchable thermoelectric generator. *Micromachines*. 2020;11(3):263.
32. Wang DF, Wang YQ, Qian ZH, Tachi T, Chuang KC. A graded Miura-ori phononic crystals lens. *Phys Lett A*. 2021;418:127701.
33. Geddes L, Pearce J, Bourland J, Silva L. Thermal properties of dry metal-foil dispersive electrosurgical electrodes. *J Clin Eng*. 1980;5(1):13-18.
34. Yu X, Fang H, Cui F, Cheng L, Lu Z. Origami-inspired foldable sound barrier designs. *J Sound Vib*. 2019;442:514-526.
35. Blanc MJ, Mulford RB, Jones MR, Iverson BD. Infrared visualization of the cavity effect using origami-inspired surfaces. *J Heat Transfer*. 2016;138(2):020901.
36. Mulford RB, Jones MR, Iverson BD. Net radiative heat exchange of an origami-inspired, variable emissivity surface. Paper presented at: ASTFE Thermal and Fluids Engineering Summer Conference. 2015.
37. Hong S, Shi Y, Li R, Zhang C, Jin Y, Wang P. Nature-Inspired, 3D origami solar steam generator toward near full utilization of solar energy. *ACS Appl Mater Interfaces*. 2018;10(34):28517-28524.
38. Mulford RB, Collins NS, Farnsworth MS, Jones MR, Iverson BD. Total hemispherical apparent radiative properties of the infinite V-groove with specular reflection. *Int J Heat and Mass Transfer*. 2018;124:168-176.

How to cite this article: Ahmed F, Khatamifar M, Lin W, Situ R. Thermal performance of dynamic, origami-inspired geometries: an experimental study. *Heat Transfer*. 2023; 1-18. doi:10.1002/htj.22852